ARTICLE

Th@C_2(8)-C_{84} and Th@C_s(15)-C_{84}: impact of actinide metal ions on the electronic structure of actinide endohedral metallofullerenes

Received 00th January 20xx,
Accepted 00th January 20xx

DOI: 10.1039/x0xx00000x

Tiantian Cao,‡[a,b] Qingyu Meng,‡[b] Ze Fu,‡[b] Yi Shen,[b] Yingjing Yan,[b] Qin Wang,[b] Bing Zhao,[a] Wenxia Wang,[a] Khaoula Merimi,[c] Antonio Rodríguez-Fortea,[c] Yang-Rong Yao,*[d] and Ning Chen*[b]

Two novel thorium-based endohedral metallofullerenes (EMFs), Th@C_2(8)-C_{84} and Th@C_s(15)-C_{84}, have been successfully synthesized and fully characterized by MALDI-TOF mass spectrum, single-crystal X-ray diffraction, UV-vis-NIR spectroscopy, cyclic voltammetry, and DFT computations. The molecular structures of Th@C_2(8)-C_{84} and Th@C_s(15)-C_{84} were unambiguously determined by single crystal X-ray crystallography, which differs from the previous theoretical prediction that the most stable structure among the Th@C_{84} isomers is Th@C_s(10)-C_{84}. These results, together with the previous reports of the isomers of U@C_{84}, show that the C_2(8)-C_{84} cage can only be stabilized by the encapsulation of actinide metals (U and Th). Detailed structural analysis shows that, in these structures, the encapsulated actinide atom has a unique interaction with the sumanene-type hexagon, which likely contributes to the stabilization of the endohedral molecular structures. Moreover, the two thorium-based EMFs show UV-vis-NIR spectra and redox behaviors which are notably different from those of the previously reported U@C_{84} isomers with the same carbon cages, suggesting that, different from lanthanide-based EMFs, endohedral actinide metal atoms have an important impact on the electronic structures of actinide metallofullerenes.

Introduction

Endohedral metallofullerene (EMF) molecular compounds have host-guest structures formed by encapsulating metal atoms or metal clusters into fullerene cages.[1-3] Since the discovery of La@C_{60},[4] EMFs have attracted great attention due to their unique metal-cage hybrid structures. Various EMFs have been synthesized and characterized in the past three decades, including mono-metallofullerenes (mono-MFs), di-metallofullerenes (di-MFs), tri-metallofullerenes (tri-MFs), and diverse clusterfullerenes. Originated from the intrinsic charge transfer from the encapsulated metallic units to the carbon cages, EMFs exhibit unique electronic and physicochemical properties, leading to potential applications in many fields, such as biomedicine[5], electrochemical catalysis,[6, 7] photovoltaic devices,[8] single-molecule devices,[9, 10] and single-molecule magnets.[11, 12]

It has been well recognized that the electronic properties of EMFs are generally governed by carbon cages, and the encapsulated metal ions have minor contributions to the frontier orbitals of EMFs. In particular, the carbon cage symmetry and electron transfer are crucial in determining the electronic structure of metallofullerenes. Fullerene with different isomeric structures generally pesent notably different properties. For example, for the mono-MFs with +2 electron transfer, the Sm@C_{2v}(9)-C_{82} and Sm@C_{3v}(7)-C_{82} isomers have completely different absorption spectra and redox behavior.[19] On the hand, charge transfer between the metal and the carbon cage also have significant impact on the properties of EMFs. For example, Sm^{2+}@C_{2v}(9)-C_{82}^{2-} and Y^{3+}@C_{2v}(9)-C_{82}^{3-}, though sharing the same cage isomer, demonstrate different absoption spectra and redox properties.[ref] In comparision, EMFs show similar UV-vis-NIR absorption spectra and redox behaviors if they share the same carbon cage isomer and formal charge state. For example, when trivalent metal ions, such as Y^{3+},[13] Gd^{3+},[14] Ce^{3+},[15] and Er^{3+},[16] are encapsulated in the same cage of C_{2v}(9)-C_{82}, they have almost identical absorption spectra. These results suggest that metal ion does not show major impact on the properites of EMFs.

Recently, a series of actinide-based EMFs have been intensively studied, starting from the synthesis of the first tetravalent mono-MF Th@C_{3v}(8)-C_{82}, which shows significantly different electronic properties and metal-cage interactions from those of the most extensively studied lanthanide EMFs.[20-27] Interestingly, unlike the fixed Ln^{2+} or Ln^{3+} oxidation states, the

[a] Suzhou Institute of Trade and Commerce, 287 Xuefu Road, Suzhou, 215009, China.
[b] College of Chemistry, Chemical Engineering and Materials Science, and State Key Laboratory of Radiation Medicine and Protection, Soochow University, Suzhou, Jiangsu 215123, P. R. China.
[c] Departament de Química Física i Inorgànica, Universitat Rovira i Virgili, 43007 Tarragona, Spain.
[d] Department of Materials Science and Engineering, CAS Key Laboratory of Materials for Energy Conversion, Anhui Laboratory of Advanced Photon Science and Technology, University of Science and Technology of China, Hefei 230026, China.

†Electronic Supplementary Information (ESI) available. CCDC 2277408 and 2277409. For ESI and crystallographic data in CIF or other electronic format see DOI: 10.1039/x0xx00000x

‡These authors contribute equally to this work.

*Corresponding authors.

actinides can adopt variable oxidation states depending on the structural configurations of the carbon cage. A series of theoretical and experimental studies have shown that thorium usually exhibits an oxidation state of +4 in mono-MFs,[28-32] while uranium varies from +3 to +6 due to its flexible oxidation state,[22, 24, 26, 33-35] leading to novel endo-units with much more complex electronic configurations than those of previously known lanthanide EMFs. In addition, compared to lanthanide EMFs, actinide-based EMFs show stronger metal-cage covalent interactions, which can be attributed to the contributions of the involved f-orbitals.[23] Thus, it is desirable to find out if the different actinide metal ions have major impacts on the electronic structures of actinide metallofullerenes. In addition, though a series of U-based EMFs have been reported, the study of Th-based EMFs has been relatively limited, and Th@C_{84} has never been reported experimentally. Theoretical work has been done to predict the most stable Th@C_{84},[36] but it hasn't been verified by experimental results.

Herein, we report the synthesis and characterization of two novel C_{84}-based Th mono-MFs, Th@C_2(8)-C_{84} and Th@C_s(15)-C_{84}. We found that, surprisingly, these two isomers are not the most stable structures for Th@C_{84} predicted by previous computational studies. Moreover, C_2(8)-C_{84} cage is currently stabilized only by actinide metals. In addition, the UV-vis-NIR absorption spectra and cyclic voltammograms of these two isomers significantly differ from those of the previously reported U@C_2(8)-C_{84} and U@C_s(15)-C_{84}, suggesting the major impact of encapsulated actinide metal ions on their electronic structures.

Results and discussion

Synthesis and Isolation of Th@C_{84}.

Thorium-based endohedral metallofullerenes were produced by a modified Krätschmer-Huffman direct-current (DC) arc-discharge method. Graphite rods packed with ThO_2 and graphite powder, with a Th/C molar ratio of 1/24, were vaporized in an arcing reactor chamber under a 200 Torr He atmosphere. The resulting soot containing thorium-based endohedral metallofullerenes was collected and extracted with CS_2 for 12 h. The two Th@C_{84} isomers were further isolated by multi-stage high-performance liquid chromatography (HPLC) separation processes (Fig. S1 and S2, ESI†). The purity of two Th@C_{84} isomers was confirmed by HPLC and the corresponding mass spectra, as shown in Fig. 1. In addition, the experimental isotopic distributions of the two Th@C_{84} isomers agree well with the theoretical predictions.

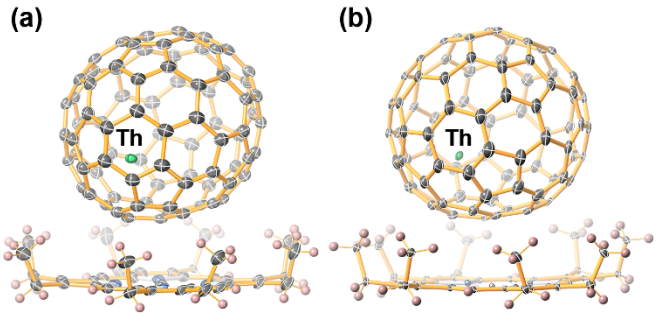

Fig. 2 Oak Ridge thermal ellipsoid plot (ORTEP) drawings of the structures of (a) Th@C_2(8)-C_{84}·[Ni^{II}(OEP)] and (b) Th@C_s(15)-C_{84}·[Ni^{II}(OEP)] with 20% thermal ellipsoids. Only the major cage orientations and primary thorium sites are illustrated. The minor metal sites and the solvent molecules are omitted for clarity.

Molecular structures of Th@C_2(8)-C_{84} and Th@C_s(15)-C_{84}.

The molecular structures of Th@C_{84} are determined by single-crystal X-ray diffraction. Briefly, the black co-crystals of two Th@C_{84} isomers and Ni^{II}(OEP) (OEP = 2, 3, 7, 8, 12, 13, 17, 18-octaethylporphyrin dianion) were obtained by diffusing the CS_2 solution of Th@C_{84} into the benzene solution of Ni^{II}(OEP). As shown in Fig. 2, the molecular structures of two Th@C_{84} isomers were unambiguously determined as Th@C_2(8)-C_{84} and Th@C_s(15)-C_{84}, respectively. The co-crystallized Ni^{II}(OEP) molecules exhibit solid π-π interactions with the EMF molecules, which are supported by the shortest Ni-C distances of 2.863 Å and 2.929 Å with Th@C_2(8)-C_{84} and Th@C_s(15)-C_{84}, respectively. Notably, the C_2(8)-C_{84} cage has only been observed in U@C_2(8)-C_{84} and has never been reported as a host cage for lanthanide endo-units. This suggests that the unique actinide-cage interactions can stabilize some uncommon carbon cages.

These two structures were resolved in the *C*2/*m* space group, commonly seen in many metallofullerene-Ni^{II}(OEP) analogs. Under this space group, the crystal structure has two orientations that are symmetrized by the crystallographic

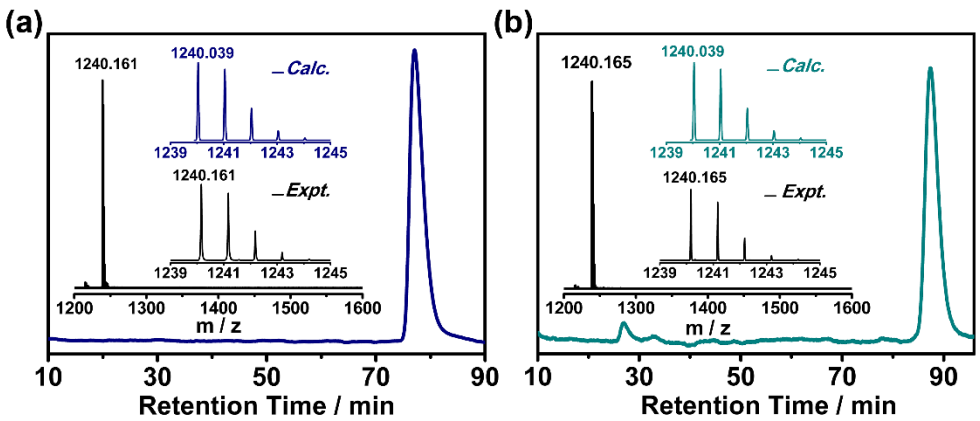

Fig. 1 HPLC chromatograms of purified (a) Th@C_2(8)-C_{84} and (b) Th@C_s(15)-C_{84} on a Buckyprep column using toluene as the eluent, with a 4 mL/min flow rate. The insets show the mass spectra of two Th@C_{84} isomers with the expansions of the experimental and calculated isotopic distributions.

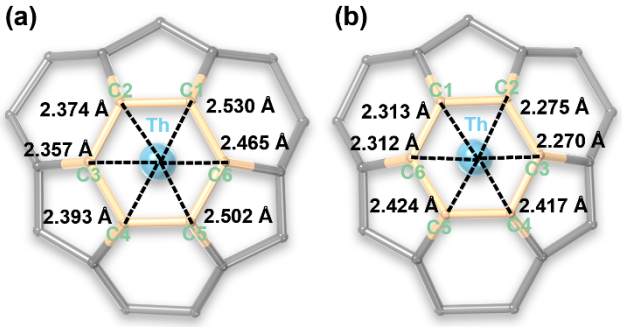

Fig. 3 Perspective drawings show the interaction of the major thorium site (marked in blue) with the closest cage portion (marked in yellow) in (a) Th@C_2(8)-C_{84} and (b) Th@C_s(15)-C_{84}, respectively.

mirror plane with equal occupancy. Accordingly, the fullerene cage with an occupancy of 0.5 is refined by combing one-half of the carbon cage with the mirror-related one-half counterpart. The crystallographic analysis shows that there are some minor disordered sites probably caused by thermal vibrations of the encapsulated Th atom in both crystal structures (Details in Fig. S3). There are five crystallographic disorder sites for the Th atom in Th@C_2(8)-C_{84}. Among them, Th1 and Th4 are both located on the crystallographic symmetry plane, and the remaining three metallic thorium sites (Th2, Th3, and Th5) generate Th2A, Th3A, and Th5A through the crystallographic mirror, respectively. The occupancy of Th1 is the highest at 0.730(3), and the occupancies of Th2 to Th5 are shown in Table S1. For Th@C_s(15)-C_{84}, there are only two crystallographic disorder sites for Th atoms. The thorium sites (Th1 and Th2) generate Th1A and Th2A by crystallographic mirroring, respectively, with the occupancies of 0.3159(10) for Th1 and 0.1841(10) for Th2. Crystallographically, we discarded the mirror-related Th1A position due to the unreasonably shortest Th1A-Cage distance of only 1.732(18) Å, similar to the case of Sc position determination in Sc$_2$@C_{3v}(8)-C_{82}.[37] Theoretically, we also considered position Th1 and discarded Th1A because the geometry optimization of the Th1A position leads to a structure with significantly higher energy than the optimization of Th1 (14 kcal·mol^{-1}). The major sites of the Th atom in both crystals have high occupancies, suggesting that the Th atoms are highly ordered inside the carbon cage. This also indicates the strong interactions between the Th atom and the carbon cage.

Fig. 3 shows the detailed geometric information between the encapsulated Th atoms and their coordinated carbon-cage patterns. Interestingly, the primary Th sites of Th@C_2(8)-C_{84} and Th@C_s(15)-C_{84} are both located below the center of a hexagon with Th-C distances in the ranges of 2.357(16)-2.530(15) Å and 2.270(18)-2.424(15) Å, respectively, as shown in Table S2. The optimized structures at the PBE0/TZP level show six Th-C distances in the ranges of 2.460-2.525 Å and 2.462-2.534 Å, respectively, which are slightly larger than in the X-ray structure and in line with previous computations on other Th@C_{2n} EMFs.[18, 22, 26-29] Furthermore, these two hexagons are surrounded by three pentagons and three hexagons, forming sumanene-type patterns. This result is similar to the previously reported U@C_2(8)-C_{84} and U@C_s(15)-C_{84},[38] and partially explains why the C_2(8)-C_{84} cage is only found in actinide metallofullerenes. Compared to lanthanide atoms, the metal-sumanene pattern is more commonly seen in actinide metallofullerenes,[38] suggesting that the encapsulated actinide atom has a unique interaction with the sumanene-type hexagon, forming a relatively stable carbon-cage fragment and thus stabilizing the whole molecule. Accordingly, An@C_2(8)-C_{84} is more favorable than Ln@C_2(8)-C_{84} due to the unique actinide-sumanene interaction supported by the theoretical predictions for the Th@C_{2n} family.[32, 39] On the other hand, the C_s(15)-C_{84} cage also prefers a single actinide atom due to the actinide-sumanene interaction, while a lanthanide cluster, such as Er_2C_2,[40] seems more favorable than a single lanthanide atom to this cage.

Straka and co-workers have studied the molecular and electronic structure of Th@C_{84} in detail by Density functional theory (DFT).[36] Their theoretical calculations indicate that the thorium atom shows a formal +4 valence state in the C_{84} cage and isomeric structure with the lowest energy calculated among the 24 IPR (isolated pentagon rule) and 110 non-IPR cage isomers based on the C_{84} cage is Th@C_s(10)-C_{84}. The encapsulation energies of Th@C_2(8)-C_{84} and Th@C_s(15)-C_{84} are significantly higher than those of Th@C_s(10)-C_{84}, which suggests that these two isomeric structures are likely unstable. However,

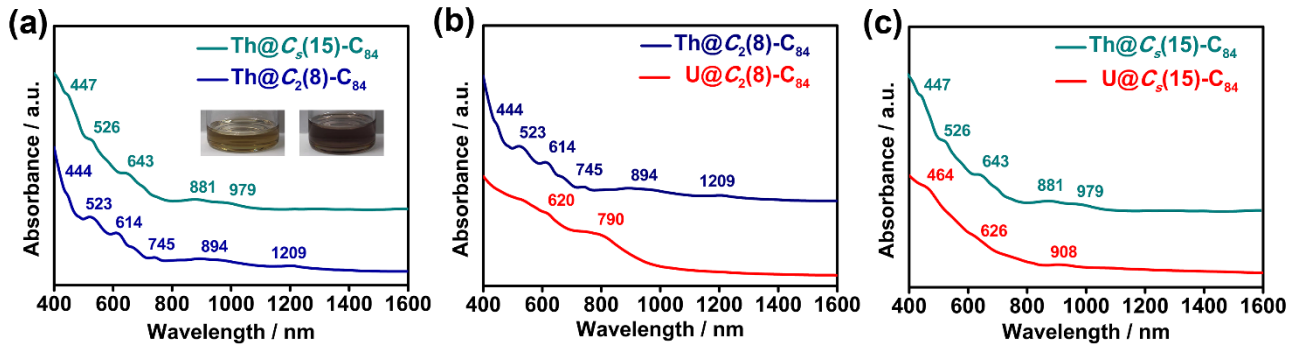

Fig. 4 (a) UV-vis-NIR absorption spectra of Th@C_2(8)-C_{84} and Th@C_s(15)-C_{84} in CS_2. The inset shows photographs of Th@C_2(8)-C_{84}(left) and Th@C_s(15)-C_{84}(right) dissolved in CS_2. UV-vis-NIR absorption spectra of (b) M@C_2(8)-C_{84} (M = Th, U) and (c) M@C_s(15)-C_{84} (M = Th, U), which share the same cage isomers. The curves are vertically shifted for ease of comparison.

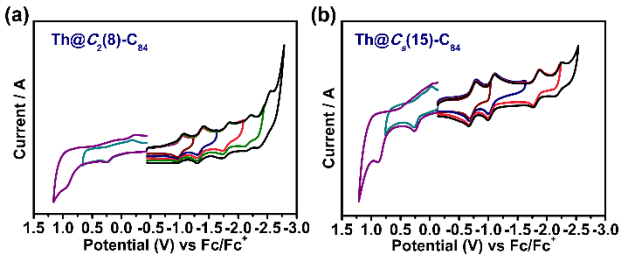

Fig. 5 Cyclic voltammograms of (a) Th@C_2(8)-C_{84} and (b) Th@C_s(15)-C_{84} in *o*-dichlorobenzene (0.05 M (*n*-Bu)$_4$NPF$_6$ as the supporting electrolyte; scan rate 100 mV/s).

in our experimental work, Th@C_2(8)-C_{84} and Th@C_s(15)-C_{84} were successfully isolated and characterized, and the predicted most stable isomer in that work, Th@C_s(10)-C_{84}, was not found in the experimentally synthesized product. This suggests that our experimental results are significantly different from the previous theoretical predictions, which indicates that theoretical calculation methods may need to be readjusted and the significant actinide-sumanene interaction needs to be considered. Indeed, when considering the thorium-sumanene interaction, isomers Th@C_2(8)-C_{84} and Th@C_s(15)-C_{84} are both lower in energy than Th@C_s(10)-C_{84} by 6.2 and 5.4 kcal·mol^{-1}, respectively, in good agreement with experiments (see Table S4 and Figure S5). Moreover, we have confirmed by inspecting the frontier molecular orbitals (Fig. S4) that the oxidation state of thorium in these two new EMFs is Th(IV), as in other mono-metallic Th@C_{2n} characterized so far.

Spectroscopic Characterizations of Th@C_2(8)-C_{84} and Th@C_s(15)-C_{84}.

Fig. 4a shows the UV-vis-NIR absorption spectra of Th@C_2(8)-C_{84} and Th@C_s(15)-C_{84} isomers dissolved in carbon disulfide (CS_2) solution. As shown in Fig. 4b, Th@C_2(8)-C_{84} exhibits six spectroscopic absorptions at 444, 523, 614, 745, 894, and 1209 nm. Such a spectrum is notably different from U@C_2(8)-C_{84}, which displays only two prominent absorption peaks at 620 and 790 nm.[38] Likewise, Th@C_s(15)-C_{84} shows five absorptions at 447, 526, 643, 881, and 979 nm, while U@C_s(15)-C_{84}, sharing the same isomeric cage structure, is featured by only three shoulder absorptions at 464, 626, and 908 nm, as shown in Fig. 4c. It is commonly acknowledged that the spectroscopic properties of EMFs are susceptible to their electronic structures, especially for the carbon cage π-system and charge state. Accordingly, EMFs sharing the same cage and isoelectronic endo-units have almost identical absorption spectra. However, in this work, the spectroscopic results clearly show that the Th@C_{84} and U@C_{84} isomers, though showing some similarities, still present remarkably different electronic structures, even though they have the same cage isomerism and charge transfer. This suggests that the contribution of the encapsulated actinide metals plays a significant role in their contribution to the corresponding molecular frontier orbitals.

Electrochemical Studies of Th@C_2(8)-C_{84} and Th@C_s(15)-C_{84}.

Fig. 5 shows the cyclic voltammograms of Th@C_2(8)-C_{84} and Th@C_s(15)-C_{84} in an *ortho*-dichlorobenzene (*o*-DCB) solution containing tetrabutylammonium hexafluorophosphate ($TBAPF_6$) as the supporting electrolyte. Th@C_2(8)-C_{84} presents two irreversible oxidation steps (+0.23 and +0.93 V) and five fully reversible reduction steps (-1.00, -1.34, -1.78, -2.16, and -2.44 V), respectively. And Th@C_s(15)-C_{84} presents two irreversible oxidation steps (+0.26 and +0.88 V) and four fully reversible reduction steps (-0.73, -1.06, -1.82, and -2.21 V), respectively. Table 1 summarizes the characteristic redox potentials of Th@C_2(8)-C_{84} and Th@C_s(15)-C_{84}, as well as those of U@C_{2n} and Th@C_{2n} (2*n* = 76, 80-86) for comparison.[20, 22, 24, 28-31, 33, 38] The first oxidation potentials of Th@C_2(8)-C_{84} (0.23 V) and Th@C_s(15)-C_{84} (0.26 V) are close to those of Th@C_{2n} (2*n* = 80, 82, 86), but have notable positive shift compared with that of Th@T_d(19151)-C_{76} (0.03 V) and negative shift compared with that of Th@C_{3v}(8)-C_{82} (0.46 V). The first reduction potentials of

Table 1. Redox potentials (V vs. Fc/Fc^+) and electrochemical band gaps of Th@C_2(8)-C_{84}, Th@C_s(15)-C_{84} and the selected reference EMFs.

Compounds	$E^{2+/+}$	$E^{+/0}$	$E^{0/-}$	$E^{-/2-}$	$E^{2-/3-}$	$E^{3-/4-}$	$E^{4-/5-}$	$E_{gap,ec}$(V)	ref
Th@C_2(8)-C_{84}	0.93[b]	0.23[b]	-1.00[a]	-1.34[a]	-1.78[a]	-2.16[a]	-2.44[a]	1.23	this work
Th@C_s(15)-C_{84}	0.88[b]	0.26[b]	-0.73[a]	-1.06[a]	-1.82[a]	-2.21[a]		0.99	this work
U@C_2(8)-C_{84}		0.08[a]	-0.75[a]	-1.32[a]	-1.64[a]	-2.22[a]		0.83	[38]
U@C_s(15)-C_{84}	0.85[a]	0.12[a]	-0.71[a]	-1.06[a]	-1.51[a]	-2.28[a]		0.83	[38]
Th@T_d(19151)-C_{76}	0.75[b]	0.03[a]	-1.04[a]	-1.41[a]	-1.78[a]	-2.19[a]		1.07	[28]
Th@D_{5h}(6)-C_{80}	0.92[b]	0.26[a]	-0.63[a]	-0.95[a]	-1.86[a]			0.89	[30]
Th@C_1(28324)-C_{80}	1.11[b]	0.24[a]	-1.22[b]	-1.50[a]	-2.05[a]	-2.14[a]		1.46	[24]
Th@C_{2v}(9)-C_{82}	0.64[b]	0.20[a]	-1.05[b]	-1.36[a]	-1.72[a]			1.25	[29]
Th@C_2(5)-C_{82}	1.01[b]	0.26[a]	-1.15[a]	-1.65[b]	-2.16[b]			1.41	[29]
Th@C_{3v}(8)-C_{82}		0.46[a]	-1.05[b]	-1.54[b]	-1.69[b]	-1.82[b]	-2.15[b]	1.51	[20]
Th@C_1(11)-C_{86}		0.21[a]	-1.17[a]	-1.51[a]	-1.85[a]	-2.24[b]		1.38	[28]
U@C_1(28324)-C_{80}		0.28[a]	-0.57[b]	-1.50[a]	-1.91[a]	-2.32[a]		0.85	[24]
U@C_2(5)-C_{82}		0.11[a]	-0.67[a]	-1.54[a]	-1.83[b]	-2.05[b]		0.78	[22]
U@C_1(11)-C_{86}		0.18[a]	-0.69[a]	-1.54[a]	-1.86[a]	-2.26[b]		0.87	[33]
U@C_{2v}(9)-C_{82}	0.92[a]	0.10[a]	-0.43[a]	-1.42[a]	-1.76[b]	-1.77[b]	-2.21[b]	0.53	[22]

[a] Half-wave potential (reversible redox process). [b] Peak potential (irreversible redox process). In all EMFs, the formal oxidation state of the actinide is An(IV), but in U@C_{2v}(9)-C_{82} is U(III).

Th@C_2(8)-C_{84} (-1.00 V) and Th@C_s(15)-C_{84} (-0.73 V) are positively shifted compared with Th@C_{2n} ($2n$ = 76, 82, 86) (-1.04, -1.22, -1.05, -1.15, -1.17 V) and Th@C_1(28324)-C_{80} (-1.22 V) and negatively shifted compared with Th@D_{5h}(6)-C_{80} (-0.63 V). Therefore, the electrochemical gaps of Th@C_2(8)-C_{84} (1.23 V) and Th@C_s(15)-C_{84} (0.99 V) are smaller than those of Th@C_{2n} ($2n$ = 82, 86) (1.25, 1.41, 1.51, and 1.38 V) and Th@C_1(28324)-C_{80} (1.46 V), and larger than those of Th@D_{5h}(6)-C_{80} (0.89 V). It is worth noting that the electrochemical reductive behavior of Th@C_2(8)-C_{84} is unique, as it shows five fully reversible reductive processes, whereas Th@C_{2n} ($2n$ = 76, 80, 82, 86) species do not have a fifth reduction step except for Th@C_{3v}(8)-C_{82} which has the fifth irreversible reduction processes. In addition, compared with uranium-based mono-EMFs sharing the same carbon cage symmetry, i.e., U@C_2(8)-C_{84} and U@C_s(15)-C_{84},[38] the first oxidation potentials of Th@C_2(8)-C_{84} (0.23 V) and Th@C_s(15)-C_{84} (0.26 V) are positively shifted while the first reduction potentials of Th@C_2(8)-C_{84} (-1.00 V) and Th@C_s(15)-C_{84} (-0.73 V) are negatively shifted, resulting in a larger electrochemical gap. This suggests that the redox behaviors of Th@C_2(8)-C_{84} and Th@C_s(15)-C_{84} also show notable differences from those of uranium-based mono-EMFs sharing the same carbon cage isomerism, indicating the essential impacts of the encapsulated actinide metals on the corresponding molecular frontier orbitals.

Conclusions

In conclusion, two novel Th@C_{84} isomers were successfully synthesized, isolated, and characterized by mass spectrometry, single-crystal X-ray diffraction, UV-vis-NIR spectroscopy, cyclic voltammetry, and DFT calculations. The molecular structures of Th@C_2(8)-C_{84} and Th@C_s(15)-C_{84} were unambiguously determined by single-crystal X-ray crystallography. Notably, these results, together with the previous reports, show that the C_2(8)-C_{84} cage can only be stabilized by the encapsulation of actinide metals (U and Th). Detailed structural analysis and computational work show that the encapsulated actinide atom has a unique interaction with the sumanene-type hexagon, forming a stable carbon-cage fragment and thus stabilizing the whole molecule. Moreover, these two isomers are found to have lower energies than the previous theoretically predicted Th@C_s(10)-C_{84}. Th@C_2(8)-C_{84} and Th@C_s(15)-C_{84} show different UV-vis-NIR absorption spectra and electrochemical behaviors from U@C_2(8)-C_{84} and U@C_s(15)-C_{84}. This indicates that the electronic structures of actinide EMFs are different from the lanthanide EMFs, whose electronic structures are largely governed by the fullerene cages. Instead, different endohedral actinide metal atoms (U and Th) have important impacts on their electronic structures, likely due to stronger actinide-cage carbon covalent interactions. This work highlights the significant impact of the endohedral actinide metal ions on the electronic structures of actinide EMFs and paves the way to the further in-depth computational study of the electronic structure of actinide-based EMFs.

Experimental

Synthesis and isolation of two Th@C_{84} isomers.

The carbon soot containing thorium EMFs was synthesized by the direct-current arc discharge method. The graphite rods, packed with ThO_2 and graphite powders (1:24 molar ratio), were vaporized in the arcing chamber under a 200 Torr He atmosphere. On average, 2 g of graphite powder and 1.84 g of ThO_2 were packed in each rod, and ca. 30 mg of crude fullerene mixture per rod was obtained. A total of 200 carbon rods were vaporized in this work, producing ca. 0.15 mg Th@C_2(8)-C_{84} and ca. 0.18 mg Th@C_s(15)-C_{84}. This experimental condition was accompanied by the synthesis of thorium-based metallofullerenes ThC_2@C_{82}. The resulting soot was refluxed in CS_2 under an argon atmosphere for 12 h. The separation and purification of the two Th@C_{84} isomers were achieved by multi-stage HPLC procedures. Multiple HPLC columns, including a Buckyprep-M column (25 × 250 mm, Cosmosil, Nacalai Tesque Inc., Japan), a Buckyprep-D column (10 × 250 mm, Cosmosil, Nacalai Tesque Inc., Japan), a 5PPB column (10 × 250 mm, Cosmosil, Nacalai Tesque Inc., Japan), and a Buckprep column (10 × 250 mm, Cosmosil, Nacalai Tesque Inc., Japan), were utilized in the procedures. Further details are described in the Supporting Information.

Spectroscopic and Electrochemical Studies.

The positive-ion mode matrix-assisted laser desorption ionization time-of-flight (MALDI-TOF) (Bruker, Germany) was employed for the mass characterization. The Vis-NIR spectra of the purified Th@C_{84} isomers dissolved in CS_2 solution were measured using a Cary 5000 UV-vis-NIR spectrophotometer (Agilent, USA). The cyclic voltammetry was obtained in *o*-DCB using a CHI-660E electrochemical workstation. A conventional three-electrode cell consisting of a platinum counter-electrode, a glassy carbon working electrode, and a silver reference electrode using a 0.05 M (n-Bu)$_4$NPF$_6$ solution as the supporting electrolyte was used for the measurements with a scan rate of 100 mV/s.

X-ray Crystallographic Study.

The black block co-crystals were obtained by slow diffusion of the CS_2 solution of Th@C_{84} into the benzene solution of [Ni^{II}(OEP)]. Single-crystal X-ray data of Th@C_2(8)-C_{84} and Th@C_s(15)-C_{84} were collected at 122 K and 120 K, respectively, on a diffractometer (APEX II; Bruker Analytik GmbH) equipped with a CCD collector. The multiscan method was used for absorption correction. The crystallographic structures of two Th@C_{84} isomers were solved and refined using SHELXT-2014 by the intrinsic phasing methods[41] and SHELXL-2018 by full-matrix least-squares based on F_2.[42]

Crystal data for C128 H51 N4 Ni Th: Mr = 1935.47, 0.1 mm × 0.08 mm × 0.06 mm, monoclinic, $C2/m$ (No. 12), a = 27.462(2) Å, b = 16.9912(14) Å, c = 17.7357(14) Å, α = 90°, β = 107.907(4)°, γ = 90°, V = 7874.7(11) Å^3, Z = 4, ρ_{calcd} = 1.633 g cm^{-3}, μ(Ga Kα) = 5.681 mm^{-1}, ϑ = 2.699-54.097, T = 122(2) K, R_1 = 0.1069, wR_2 =0.2168 for all data; R_1 = 0.0719, wR_2 =0.1922 for 4838 reflections ($I > 2.0\sigma(I)$) with 1031 parameters. Goodness-of-fit indicator 1.029. Maximum residual electron density 0.793 e Å^{-3}.

Crystal data for Th@C_s(15)-C_{84}·$C_{36}H_{44}N_4Ni$·C_6H_6: Mr = 1910.45, 0.14 mm × 0.1 mm × 0.06 mm, monoclinic, $C2/m$ (No. 12), a = 25.3891(17) Å, b = 15.1408(11) Å, c = 19.9283(14) Å, α = 90°, β = 94.674(4)°, γ = 90°, V = 7635.5(9) Å^3, Z = 4, ρ_{calcd} = 1.662 g cm^{-3}, μ(Ga Kα) = 5.853 mm^{-1}, ϑ = 1.935-53.946, T = 120(2) K, R_1 = 0.1237, wR_2 = 0.2660 for all data; R_1 = 0.0921, wR_2 = 0.2444 for 5073 reflections ($I > 2.0\sigma(I)$) with 999 parameters. Goodness-of-fit indicator 1.057. Maximum residual electron density 1.198 e Å^{-3}.

The crystallographic data for these two structures have been deposited at the Cambridge Crystallographic Data Centre (CCDC) with the deposition numbers 2277408 and 2277409.

Computational Details.

Calculations were carried out using density functional theory (DFT) with the ADF 2019 package using PBE0 functional.[43, 44] Slater triple-zeta polarization (TZP) basis sets were used to describe the valence electrons of Th and C. Frozen cores were described by means of single Slater functions, consisting of the 1s shell for C, the 1s to 5d shells for U and Th. Scalar relativistic corrections were included by means of the ZORA formalism. Dispersion corrections by Grimme were also included.[45]

Conflicts of interest

There are no conflicts to declare.

Acknowledgements

N. C. thanks the National Science Foundation China (NSFC 52172051), the Natural Science Foundation of Jiangsu Province (BK20200041, BK20221247), the Natural Science Foundation of the Jiangsu Higher Education Institutions of China (22KJD430008), and the Priority Academic Program Development of Jiangsu Higher Education Institutions (PAPD). Qingyu Meng thanks Postgraduate Research & Practice Innovation Program of Jiangsu Province (KYCX23_3230). The Fundamental Research Funds for the Central Universities (WK2060000051). A.R.-F. thanks the Spanish Ministry of Science and Innovation (grant PID2020-112762GB-I00 funded by MCIN/AEI/10.13039/501100011033), the Generalitat de Catalunya (grant 2021SGR00110), and the URV for support.

Notes and references

1 L. Bao, P. Peng and X. Lu, Bonding inside and outside Fullerene Cages, *Acc. Chem. Res.*, 2018, **51**, 810-815.
2 X. Lu, L. Feng, T. Akasaka and S. Nagase, Current status and future developments of endohedral metallofullerenes, *Chem. Soc. Rev.*, 2012, **41**, 7723-7760.
3 A. A. Popov, S. Yang and L. Dunsch, Endohedral Fullerenes, *Chem. Rev.*, 2013, **113**, 5989-6113.
4 J. R. Heath, S. C. O'Brien, Q. Zhang, Y. Liu, R. F. Curl, F. K. Tittel and R. E. Smalley, Lanthanum complexes of spheroidal carbon shells, *J. Am. Chem. Soc.*, 1985, **107**, 7779-7780.

5 Y. Liu, C. Chen, P. Qian, X. Lu, B. Sun, X. Zhang, L. Wang, X. Gao, H. Li, Z. Chen, J. Tang, W. Zhang, J. Dong, R. Bai, P. E. Lobie, Q. Wu, S. Liu, H. Zhang, F. Zhao, M. S. Wicha, T. Zhu and Y. Zhao, Gd-metallofullerenol nanomaterial as non-toxic breast cancer stem cell-specific inhibitor, *Nat. Commun.*, 2015, **6**, 5988.

6 A. R. Puente Santiago, M. F. Sanad, A. Moreno-Vicente, M. A. Ahsan, M. R. Cerón, Y.-R. Yao, S. T. Sreenivasan, A. Rodriguez-Fortea, J. M. Poblet and L. Echegoyen, A New Class of Molecular Electrocatalysts for Hydrogen Evolution: Catalytic Activity of $M_3N@C_{2n}$ (2n = 68, 78, and 80) Fullerenes, *J. Am. Chem. Soc.*, 2021, **143**, 6037-6042.

7 J. Zheng, L. Huang, C.-H. Cui, Z.-C. Chen, X.-F. Liu, X. Duan, X.-Y. Cao, T.-Z. Yang, H. Zhu, K. Shi, P. Du, S.-W. Ying, C.-F. Zhu, Y.-G. Yao, G.-C. Guo, Y. Yuan, S.-Y. Xie and L.-S. Zheng, Ambient-pressure synthesis of ethylene glycol catalyzed by C_{60}-buffered Cu/SiO_2, *Science*, 2022, **376**, 288-292.

8 W. Li, F. Qu, L. Liu, Z. Zhang, J. Liang, Y. Lu, J. Zhang, L. Wang, C. Wang and T. Wang, A Metallofullertube of $Ce_2@C_{100}$ with a Carbon Nanotube Segment: Synthesis, Single-Molecule Conductance and Supramolecular Assembly, *Angew. Chem. Int. Ed.*, 2022, **61**, e202116854.

9 K. Zhang, C. Wang, M. Zhang, Z. Bai, F.-F. Xie, Y.-Z. Tan, Y. Guo, K.-J. Hu, L. Cao, S. Zhang, X. Tu, D. Pan, L. Kang, J. Chen, P. Wu, X. Wang, J. Wang, J. Liu, Y. Song, G. Wang, F. Song, W. Ji, S.-Y. Xie, S.-F. Shi, M. A. Reed and B. Wang, A $Gd@C_{82}$ single-molecule electret, *Nat. Nanotechnol.*, 2020, **15**, 1019-1024.

10 J. Li, S. Hou, Y.-R. Yao, C. Zhang, Q. Wu, H.-C. Wang, H. Zhang, X. Liu, C. Tang, M. Wei, W. Xu, Y. Wang, J. Zheng, Z. Pan, L. Kang, J. Liu, J. Shi, Y. Yang, C. J. Lambert, S.-Y. Xie and W. Hong, Room-temperature logic-in-memory operations in single-metallofullerene devices, *Nat. Mater.*, 2022, **21**, 917-923.

11 F. Liu, D. S. Krylov, L. Spree, S. M. Avdoshenko, N. A. Samoylova, M. Rosenkranz, A. Kostanyan, T. Greber, A. U. B. Wolter, B. Büchner and A. A. Popov, Single molecule magnet with an unpaired electron trapped between two lanthanide ions inside a fullerene, *Nat. Commun.*, 2017, **8**, 16098.

12 F. Liu, G. Velkos, D. S. Krylov, L. Spree, M. Zalibera, R. Ray, N. A. Samoylova, C.-H. Chen, M. Rosenkranz, S. Schiemenz, F. Ziegs, K. Nenkov, A. Kostanyan, T. Greber, A. U. B. Wolter, M. Richter, B. Büchner, S. M. Avdoshenko and A. A. Popov, Air-stable redox-active nanomagnets with lanthanide spins radical-bridged by a metal–metal bond, *Nat. Commun.*, 2019, **10**, 571.

13 K. Kikuchi, Y. Nakao, S. Suzuki, Y. Achiba, T. Suzuki and Y. Maruyama, Characterization of the Isolated $Y@C_{82}$, *J. Am. Chem. Soc.*, 1994, **116**, 9367-9368.

14 M. Suzuki, X. Lu, S. Sato, H. Nikawa, N. Mizorogi, Z. Slanina, T. Tsuchiya, S. Nagase and T. Akasaka, Where Does the Metal Cation Stay in $Gd@C_{2v}(9)$-C_{82}? A Single-Crystal X-ray Diffraction Study, *Inorg. Chem.*, 2012, **51**, 5270-5273.

15 M. Suzuki, M. Yamada, Y. Maeda, S. Sato, Y. Takano, F. Uhlík, Z. Slanina, Y. Lian, X. Lu, S. Nagase, M. M. Olmstead, A. L. Balch and T. Akasaka, The Unanticipated Dimerization of $Ce@C_{2v}(9)$-C_{82} upon Co-crystallization with Ni(octaethylporphyrin) and Comparison with Monomeric $M@C_{2v}(9)$-C_{82} (M = La, Sc, and Y), *Chem. - Eur. J.*, 2016, **22**, 18115-18122.

16 S. Hu, T. Liu, W. Shen, Z. Slanina, T. Akasaka, Y. Xie, F. Uhlik, W. Huang and X. Lu, Isolation and Structural Characterization of $Er@C_{2v}(9)$-C_{82} and $Er@C_s(6)$-C_{82}: Regioselective Dimerization of a Pristine Endohedral Metallofullerene Induced by Cage Symmetry, *Inorg. Chem.*, 2019, **58**, 2177-2182.

17 B.-Y. Sun, T. Inoue, T. Shimada, T. Okazaki, T. Sugai, K. Suenaga and H. Shinohara, Synthesis and Characterization of Eu-Metallofullerenes from $Eu@C_{74}$ to $Eu@C_{90}$ and Their Nanopeapods, *J. Phys. Chem. B*, 2004, **108**, 9011-9015.

18 X. Lu, Z. Slanina, T. Akasaka, T. Tsuchiya, N. Mizorogi and S. Nagase, $Yb@C_{2n}$ (n = 40, 41, 42): New Fullerene Allotropes with Unexplored Electrochemical Properties, *J. Am. Chem. Soc.*, 2010, **132**, 5896-5905.

19 Z. Hu, Y. Hao, Z. Slanina, Z. Gu, Z. Shi, F. Uhlík, Y. Zhao and L. Feng, Popular C_{82} Fullerene Cage Encapsulating a Divalent Metal Ion Sm^{2+}: Structure and Electrochemistry, *Inorg. Chem.*, 2015, **54**, 2103-2108.

20 Y. Wang, R. Morales-Martínez, X. Zhang, W. Yang, Y. Wang, A. Rodríguez-Fortea, J. M. Poblet, L. Feng, S. Wang and N. Chen, Unique Four-Electron Metal-to-Cage Charge Transfer of Th to a C_{82} Fullerene Cage: Complete Structural Characterization of $Th@C_{3v}(8)$-C_{82}, *J. Am. Chem. Soc.*, 2017, **139**, 5110-5116.

21 P. Zhao, X. Zhao and M. Ehara, Theoretical Insights into Monometallofullerene $Th@C_{76}$: Strong Covalent Interaction between Thorium and the Carbon Cage, *Inorg. Chem.*, 2018, **57**, 2961-2964.

22 W. Cai, R. Morales-Martínez, X. Zhang, D. Najera, E. L. Romero, A. Metta-Magaña, A. Rodríguez-Fortea, S. Fortier, N. Chen, J. M. Poblet and L. Echegoyen, Single crystal structures and theoretical calculations of uranium endohedral metallofullerenes ($U@C_{2n}$, 2n = 74, 82) show cage isomer dependent oxidation states for U, *Chem. Sci.*, 2017, **8**, 5282-5290.

23 Y. Li, L. Yang, C. Liu, Q. Hou, P. Jin and X. Lu, Th-Based Endohedral Metallofullerenes: Anomalous Metal Position and Significant Metal-Cage Covalent Interactions with the Involvement of Th 5f Orbitals, *Inorg. Chem.*, 2018, **57**, 7142-7150.

24 W. Cai, L. Abella, J. Zhuang, X. Zhang, L. Feng, Y. Wang, R. Morales-Martínez, R. Esper, M. Boero, A. Metta-Magaña, A. Rodríguez-Fortea, J. M. Poblet, L. Echegoyen and N. Chen, Synthesis and Characterization of Non-Isolated-Pentagon-Rule Actinide Endohedral Metallofullerenes $U@C_1(17418)$-C_{76}, $U@C_1(28324)$-C_{80}, and $Th@C_1(28324)$-C_{80}: Low-Symmetry Cage Selection Directed by a Tetravalent Ion, *J. Am. Chem. Soc.*, 2018, **140**, 18039-18050.

25 K. Akiyama, Y. Zhao, K. Sueki, K. Tsukada, H. Haba, Y. Nagame, T. Kodama, S. Suzuki, T. Ohtsuki, M. Sakaguchi, K. Kikuchi, M. Katada and H. Nakahara, Isolation and Characterization of Light Actinide Metallofullerenes, *J. Am. Chem. Soc.*, 2001, **123**, 181-182.

26 X. Zhang, W. Li, L. Feng, X. Chen, A. Hansen, S. Grimme, S. Fortier, D.-C. Sergentu, T. J. Duignan, J. Autschbach, S. Wang, Y. Wang, G. Velkos, A. A. Popov, N. Aghdassi, S. Duhm, X. Li, J. Li, L. Echegoyen, W. H. E. Schwarz and N. Chen, A diuranium carbide cluster stabilized inside a C_{80} fullerene cage, *Nat. Commun.*, 2018, **9**, 2753.

27 Y. Shen, X. Yu, Q. Meng, Y.-R. Yao, J. Autschbach and N. Chen, $ThC_2@C_{82}$ versus $Th@C_{84}$: unexpected formation of triangular thorium carbide cluster inside fullerenes, *Chem. Sci.*, 2022, **13**, 12980-12986.

28 M. Jin, J. Zhuang, Y. Wang, W. Yang, X. Liu and N. Chen, $Th@T_d(19151)$-C_{76}: A Highly Symmetric Fullerene Cage Stabilized by a Tetravalent Actinide Metal Ion, *Inorg. Chem.*, 2019, **58**, 16722-16726.

29 Q. Meng, R. Morales-Martínez, J. Zhuang, Y.-R. Yao, Y. Wang, L. Feng, J. M. Poblet, A. Rodríguez-Fortea and N. Chen, Synthesis and Characterization of Two Isomers of $Th@C_{82}$: $Th@C_{2v}(9)$-C_{82} and $Th@C_2(5)$-C_{82}, *Inorg. Chem.*, 2021, **60**, 11496-11502.

30 Y. Yan, R. Morales-Martínez, J. Zhuang, Y.-R. Yao, X. Li, J. M. Poblet, A. Rodríguez-Fortea and N. Chen, $Th@D_{5h}(6)$-C_{80}: a highly symmetric fullerene cage stabilized by a single metal ion, *Chem. Commun.*, 2021, **57**, 6624-6627.

31 Y. Wang, R. Morales-Martínez, W. Cai, J. Zhuang, W. Yang, L. Echegoyen, J. M. Poblet, A. Rodríguez-Fortea and N. Chen, $Th@C_1(11)$-C_{86}: an actinide encapsulated in an unexpected C_{86} fullerene cage, *Chem. Commun.*, 2019, **55**, 9271-9274.

32 Y. Li, L. Yang, Z. Wei, Q. Hou, L. Li and P. Jin, Robust metal-pentagon interactions in the Th-based endohedral metallofullerenes revealed by DFT calculations, *Int. J. Quantum Chem.*, 2019, **119**, e25826.

33 W. Cai, J. Alvarado, A. Metta-Magaña, N. Chen and L. Echegoyen, Interconversions between Uranium Mono-metallofullerenes: Mechanistic Implications and Role of Asymmetric Cages, *J. Am. Chem. Soc.*, 2020, **142**, 13112-13119.

34 X. Zhang, Y. Wang, R. Morales-Martínez, J. Zhong, C. de Graaf, A. Rodríguez-Fortea, J. M. Poblet, L. Echegoyen, L. Feng and N. Chen, $U_2@I_h(7)$-C_{80}: Crystallographic Characterization of a Long-Sought Dimetallic Actinide Endohedral Fullerene, *J. Am. Chem. Soc.*, 2018, **140**, 3907-3915.

35 A. Moreno-Vicente, M. Alías-Rodríguez, P. W. Dunk, C. de Graaf, J. M. Poblet and A. Rodríguez-Fortea, Highly oxidized U(vi) within the smallest fullerene: gas-phase synthesis and computational study of boron-doped U@C_{27}B, *Inorg. Chem. Front.*, 2023, **10**, 908-914.

36 J. Kaminský, J. Vícha, P. Bouř and M. Straka, Properties of the Only Thorium Fullerene, Th@C_{84}, Uncovered, *J. Phys. Chem. A*, 2017, **121**, 3128-3135.

37 Y.-R. Yao, X.-M. Shi, S.-Y. Zheng, Z.-C. Chen, S.-Y. Xie, R.-B. Huang and L.-S. Zheng, Atomically Precise Insights into Metal–Metal Bonds Using Comparable Endo-Units of Sc_2 and Sc_2C_2, *CCS Chem.*, 2021, **3**, 294-302.

38 Y.-R. Yao, Y. Roselló, L. Ma, A. R. Puente Santiago, A. Metta-Magaña, N. Chen, A. Rodríguez-Fortea, J. M. Poblet and L. Echegoyen, Crystallographic Characterization of U@C_{2n} (2n = 82-86): Insights about Metal-Cage Interactions for Mono-metallofullerenes, *J. Am. Chem. Soc.*, 2021, **143**, 15309-15318.

39 Y.-X. Gu, H. Zheng, D.-H. Li and X. Zhao, M@C_{78} (M = U, Th): Inherent Topological Connectivity Existed in Thermodynamically Stable Isomers and the Possibility of an Endohedral Fullerene Containing One Heptagon Ring, *J. Phys. Chem. A*, 2023, **127**, 6012-6019.

40 S. Hu, P. Zhao, W. Shen, M. Ehara, Y. Xie, T. Akasaka and X. Lu, Crystallographic Characterization of Er_2C_2@$C_{80\text{-}88}$: Cluster Stretching with Cage Elongation, *Inorg. Chem.*, 2020, **59**, 1940-1946.

41 O. V. Dolomanov, L. J. Bourhis, R. J. Gildea, J. A. K. Howard and H. Puschmann, $OLEX_2$: a complete structure solution, refinement and analysis program, *J. Appl. Crystallogr.*, 2009, **42**, 339-341.

42 G. Sheldrick, Crystal structure refinement with SHELXL, *Sect. C: Struct. Chem.*, 2015, **71**, 3-8.

43 G. te Velde, F. M. Bickelhaupt, E. J. Baerends, C. Fonseca Guerra, S. J. A. van Gisbergen, J. G. Snijders and T. Ziegler, Chemistry with ADF, *J. Comput. Chem.*, 2001, **22**, 931-967.

44 M. Ernzerhof and G. E. Scuseria, Assessment of the Perdew–Burke–Ernzerhof exchange-correlation functional, *J. Chem. Phys.*, 1999, **110**, 5029-5036.

45 S. Grimme, S. Ehrlich and L. Goerigk, Effect of the damping function in dispersion corrected density functional theory, *J. Comput. Chem.*, 2011, **32**, 1456-1465.